Non-singular dislocation fields

2009 IOP Conf. Ser.: Mater. Sci. Eng. 3 012026

(http://iopscience.iop.org/1757-899X/3/1/012026)

IOP Conf. Series: Materials Science and Engineering **3** (2009) 012026 doi:10.1088/1757-899X/3/1/012026

Non-singular dislocation fields

Elias C. Aifantis

Laboratory of Mechanics and Materials, Faculty of Engineering, Aristotle University of Thessaloniki, GR-54124, Thessaloniki, Greece

and

Center for Mechanics of Materials, Michigan Technological University, Houghton MI 49931, USA

mom@mom.gen.auth.gr

Abstract. Non-singular solutions for dislocation and disclination fields have recently been obtained by the author and his co-workers by using a robust model of gradient elasticity theory. These solutions, whose form is simple and easy to implement, are obtained by reducing the gradient elasticity problem to a corresponding linear elasticity boundary value problem through the solutions of an inhomogeneous Helmholtz equation where the source term is the classical singular solution. The Laplacian in the Helmholtz equation, involving the extra gradient coefficient, produces a new term in the gradient solution which asymptotically approaches the negative of the classical elasticity solution on the dislocation line. Thus, the singularity is eliminated and an arbitrary estimate of the dislocation core size introduced in classical theory, is not required. These predictions are tested against atomistic calculations and their implications to various dislocation related configurations are discussed. Due to the simple and elegant form of these solutions, it is hoped that they will be useful in discrete dislocation dynamics simulations.

1. Introduction

Higher-order elasticity theories have been introduced as early as in the 18th Century (Cauchy, Voigt) and later in the 19th Century (brothers Cosserat) as discussed briefly in [1]. In the 1960's-70's period, a large number of significant contributions were made in this field (Toupin, Rivlin, Mindlin, Kroner, Kunin, Eringen) with most notable among them, for the present purposes, the 1965 Mindlin's strain gradient theory. For a literature account of these early contributions the reader may consult [1] and the references quoted therein. These theories, in their most general form, included a prohibitively large number of constants (sometimes over 1000) and the solution of boundary value problems was not a realistic task to undertake. Most of them were worked out for wave propagation studies and for modeling dispersion effects. Even the famous - and still popular today - Mindlin's simplest theory involved 5 new constants which were not only difficult to evaluate but they were also competing each other without being able, among other things, to eliminate singularities from dislocation fields.

It was not until 1992 that this task was conveniently accomplished through the author's gradient elasticity theory (Gradela), involving only one new extra constant c with a direct physical interpretation. Determination of this constant (commonly known as gradient coefficient) from

atomistic models, as well as experimental data from wave propagation, size effect and finite dislocation and crack stress/strain field studies is possible, even though much more work in this direction is required. Since the author's 1992 paper [1] (for a recent review see also [2]), over 500 articles have been written in the 1995-2008 period using Gradela as a basis. Nevertheless, the solution of boundary value problems remained as a difficult task in most of these works, due to the complexity of the boundary conditions derived from variational formalisms.

A simple method to use Gradela for the solution of boundary value problems is briefly outlined in the next section.

2. Gradela's Robust Version

Following [2], we outline here the basics of Gradela as follows: It turns out that the stress and strain fields (σ,ε) can be determined from the inhomogeneous Helmholtz equations

$$\boldsymbol{\sigma} - c\nabla^2\boldsymbol{\sigma} = \boldsymbol{\sigma}^{\mathbf{0}} \quad ; \qquad \boldsymbol{\varepsilon} - c\nabla^2\boldsymbol{\varepsilon} = \boldsymbol{\varepsilon}^{\mathbf{0}}, \tag{1}$$

where $(\boldsymbol{\sigma}^{\mathbf{0}},\boldsymbol{\varepsilon}^{\mathbf{0}})$ are the macroscopic fields and $(\boldsymbol{\sigma},\boldsymbol{\varepsilon})$ are the local gradient-dependent fields. The macroscopic fields $(\boldsymbol{\sigma}^{\mathbf{0}},\boldsymbol{\varepsilon}^{\mathbf{0}})$ are determined from the classical constitutive equation of Hooke's law

$$\boldsymbol{\sigma}^{\mathbf{0}} = \left(\lambda \mathrm{tr}\boldsymbol{\varepsilon}^{\mathbf{0}}\right)\mathbf{1} + 2G\boldsymbol{\varepsilon}^{\mathbf{0}}, \tag{2}$$

where (λ, G) are the Lamé constants. The derivation of Eq. (1) from the general gradient elasticity theory is established by adopting a procedure similar to that of Ru and Aifantis [3] but a more robust and direct procedure is possible as discussed elsewhere.

The solution of boundary value problems now proceeds as follows: First we determine $(\boldsymbol{\sigma}^{\mathbf{0}},\varepsilon^{\mathbf{0}})$ from classical elasticity and the corresponding boundary value problem. Next we determine $(\boldsymbol{\sigma},\boldsymbol{\varepsilon})$ from the inhomogeneous Helmholtz equation with "self-consistent" boundary conditions; a task which will also be discussed, in general, elsewhere. In the next section we give a direct application of the method to determine the stress and strain field of a screw dislocation.

3. Screw Dislocation

On the basis of Eq. (1) we write the corresponding expression for ε_{yz} component of the strain tensor for a screw dislocation within the Gradela framework, i.e.

$$\varepsilon_{yz} - c\nabla^2\varepsilon_{yz} = \varepsilon^0_{yz}, \tag{3}$$

and express, furthermore, the solution ε_{yz} as the sum $\varepsilon_{yz} = \varepsilon^0_{yz} + \varepsilon^{\mathrm{extra}}_{yz}$. The classical term ε^0_{yz} is found from Hooke's law of Eq. (2) and the corresponding elastic boundary value problem, as $\varepsilon^0_{yz} = (b/4\pi)(\cos\theta/r) = (b/4\pi)(x/r^2)$, where b denotes Burgers vector magnitude and (r,θ) are the usual polar coordinates. Upon substitution of the preceding two expressions in Eq. (3) we obtain

$$\varepsilon^{\mathrm{extra}}_{yz} - c\Delta\varepsilon^{\mathrm{extra}}_{yz} = 0. \tag{4}$$

In general, the above (homogeneous) Helmholtz equation admits solutions, through the separation of variables technique, of the form

$$\varepsilon^{\mathrm{extra}}_{yz} = \left(A\cos\sqrt{n}\theta + B\sin\sqrt{n}\theta\right)\left[\Gamma I_{\sqrt{n}}\left(\frac{r}{\sqrt{c}}\right) + \Delta K_{\sqrt{n}}\left(\frac{r}{\sqrt{c}}\right)\right]. \tag{5}$$

where (I,K) denote modified Bessel functions of the first and second kind, respectively, and (A,B,Γ,Δ) are constants. By imposing the condition $\lim_{r\to\infty}\varepsilon^{\mathrm{extra}}_{yz} = 0$, we have $\Gamma = 0$. Moreover, in view of the symmetries involved in the present configuration of a screw dislocation, we may set B=0 and n=1. Next we note that the condition $\lim_{r\to 0}\varepsilon_{yz} = 0$ implies $A\Delta = -b/4\pi\sqrt{c}$, since $\lim_{r\to 0} K_1\left(r/\sqrt{c}\right) = \sqrt{c}/r$. Thus, we find that $\varepsilon^{\mathrm{extra}}_{yz} = [-b/(4\pi\sqrt{c})]K_1(r/\sqrt{c})\cos\theta$ and, therefore,

$$\varepsilon_{yz}=\frac{b}{4\pi}\left[\frac{x}{r^2}-\frac{x}{r\sqrt{c}}K_1\left(\frac{r}{\sqrt{c}}\right)\right] \quad \text{or} \quad \varepsilon_{yz}=\frac{b\cos\theta}{4\pi}\left[\frac{1}{r}-\frac{1}{\sqrt{c}}K_1\left(\frac{r}{\sqrt{c}}\right)\right]. \tag{6}$$

We note again that for $r\to 0$, $K_1\left(r/\sqrt{c}\right)\to\sqrt{c}/r$ and, thus, ε_{yz} vanishes on the dislocation line. Similar expressions we obtain easily for ε_{xz} and the corresponding stress components, as well as for the strain energy.

4. Dislocation Self-Energies

Partial dislocations in Wurtzite GaN were considered [4] though continuum and atomistic calculations by using respectively gradient elasticity and a modified Stillinger-Weber potential of the form

$$V_2\left(r_{ij}\right)=\begin{cases}k\alpha\left[\beta\left(r_{ij}/\ell\right)^{-4}-1\right]e^{\left(r_{ij}/\ell-d\right)^{-1}}, & r_{ij}/\ell<d\\ 0, & r_{ij}/\ell\geq d\end{cases}\quad;\quad 2-\text{body term}, \tag{7}$$

and

$$V_3\left(r_{ij},r_{ik},\theta_{ijk}\right)=k\gamma\, e^{\delta\left(r_{ij}-d\right)^{-1}+\delta\left(r_{ik}-d\right)^{-1}}\left(\cos\theta_{ijk}+\theta_0\right)^2 \quad;\quad 3-\text{body term}, \tag{8}$$

where the various coefficients are constants and the rest of the symbols have their usual meaning (see, for example, [4c] for details of atomistics). Figure 1a shows a partial $b_e=1/6\langle 20\bar{2}3\rangle$ edge dislocation in GaN. The GaN structure involves 2 hcp superlattices with lattice constants $a\approx 3.2\,\text{Å}$, and $a'\approx 5.2\,\text{Å}$. The far displacement field was computed by using anisotropic elasticity and the calculation of energies was established first for each atom (V^i) and then for a supercell ($V^S=\sum V^i$) involving 16000 atoms. The quench molecular dynamics method of Verlet [5] was employed with periodic boundary conditions and the defect energy was calculated from the formula $W_d=V^S_{\text{Dislocated}}-V^S_{\text{Perfect}}$. Figure 1b shows the simulation results for the self-energy W stored in a region bounded by a cylinder of radius R for an edge partial dislocation delineating a I_1 stacking fault formed by a precipitated interstitial loop. [Large symbols denote N-polarity, whereas small symbols denote Ga-polarity.]

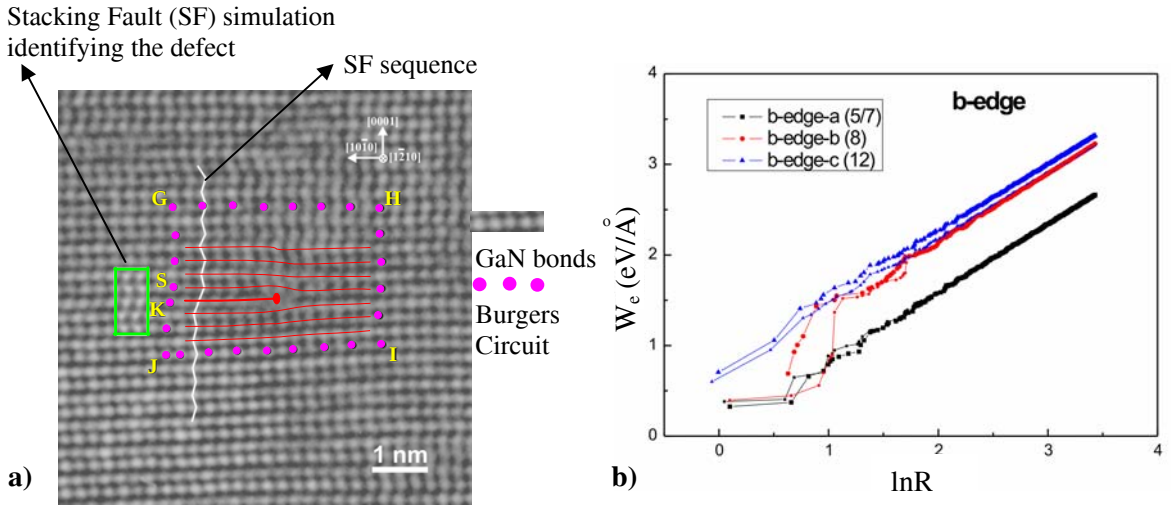

Figure 1: a) *GaN dislocated supercell*; **b)** *Self-energy W stored in a cylindrical region of radius R for edge partial dislocations*

Figure 2 shows the plots of the corresponding analytical results obtained from Gradela based on the relevant strain energy expression. This expression is non-singular and reads

$$W = \frac{Gb^2}{4\pi(1-\nu)}\left\{\ln\frac{R}{2\sqrt{c}} + \gamma^E + \frac{1}{2} + 2K_0\left(\frac{R}{\sqrt{c}}\right) + 2\frac{\sqrt{c}}{R}K_1\left(\frac{R}{\sqrt{c}}\right) - \frac{2c}{R^2}\right\}, \quad (9)$$

which for $R \to \infty$ reduces to the simpler expression $W = \frac{Gb^2}{4\pi(1-\nu)}\left\{\ln\frac{R}{2\sqrt{c}} + \gamma^E + \frac{1}{2}\right\}$, where $\gamma^E = 0.577...$ denotes the Euler's constant. [It should be noted that the term $1/2$ in this last expression and a corresponding term in Eq. (9) should be replaced, in general, with a term which depends on the Poisson's ratio. This term is approximately $1/2$ for the model of Eq. (1) for an edge dislocation in the limiting case of $R \to \infty$.]

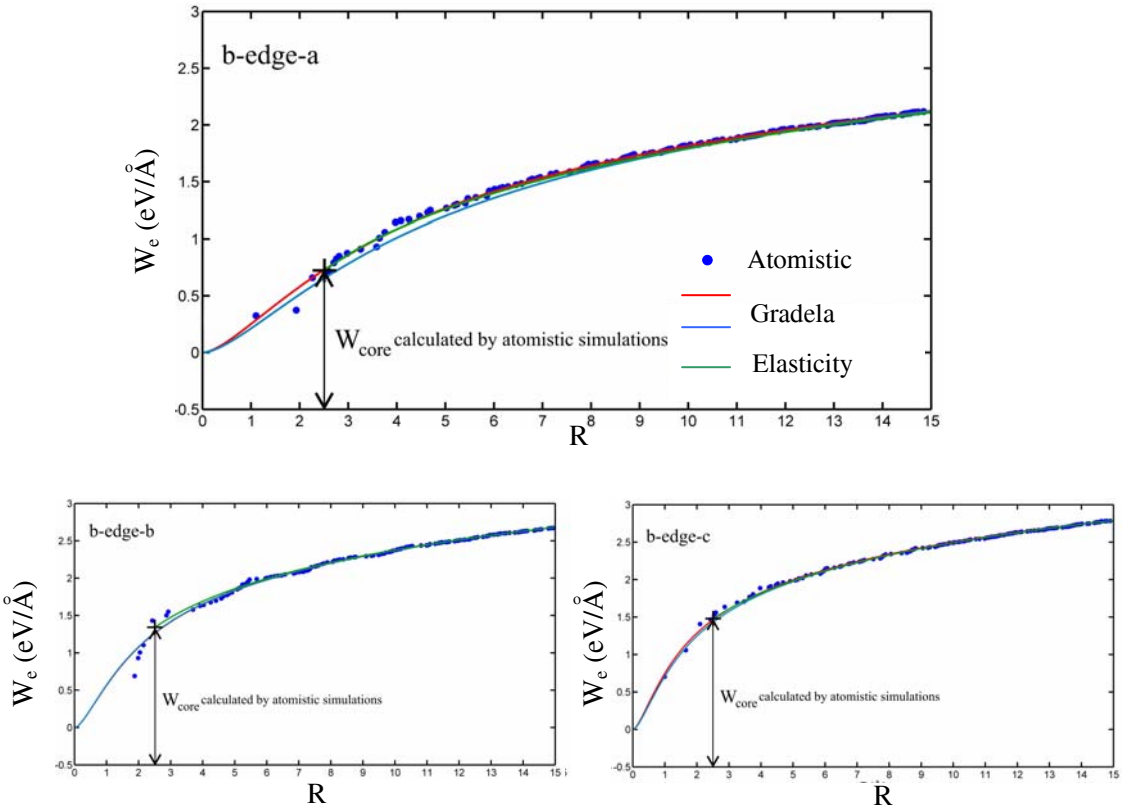

Figure 2: *Comparison of self-energy calculated from Gradela and classical elasticity for three edge partial dislocation configurations*

From these results we note that the gradient coefficient c (or internal length $\sqrt{c}$) varies in the range $c = 0.2 - 2.2$ Å^2, and the following invariant relations also hold: $W_{core}\sqrt{c}/r_0 = 0.33 \pm 0.008$ eV/Å, $W^g(b)\sqrt{c}/b = 0.3 \pm 0.008$ eV/Å. [More details on experimental and atomistic simulation considerations contained in this and the next section can be found in the articles listed in [4] as obtained by the electron microscopy group of Aristotle University.]

5. Dislocation Cores and Dislocation Density Tensor

Recently, high resolution transmission electron microscopy and image processing, along with circuit mapping techniques were used to obtain, through a Geometric Phase Analysis (GPA), dislocation core configuration. GPA enables to record the displacement fields through which we can calculate the

corresponding deformation/distortion fields and, therefore, to compare the relevant strain components and the Dislocation Density Tensor (DDT) through the familiar expression:

$$\boldsymbol{\alpha} = \nabla \times \boldsymbol{\varepsilon}; \quad \boldsymbol{\alpha} = \begin{cases} 0 & \text{outside} \perp \text{core}, \\ \neq 0 & \text{including} \perp \text{core}. \end{cases} \tag{10}$$

It is well known that elasticity theory leads again to singularities. For example, for a screw dislocation, the appropriate component of the dislocation density tensor reads $\alpha_z = b_z \delta(x)\,\delta(y)$, where b_z is the Burgers vector.

For the same dislocation configuration, application of Gradela in the form $\boldsymbol{\varepsilon} - \ell_1^2 \nabla^2 \boldsymbol{\varepsilon} = \boldsymbol{\varepsilon_0}$; $\ell_1 = \sqrt{c}$, gives $\alpha_z = b_z / (2\pi \ell_1^2) K_0(r/\ell_1)$; which is still singular, but smoother than the δ-function.

To obtain results enabling comparison with experiments we use a modified higher-order Gradela model which reads

$$\boldsymbol{\varepsilon} - \ell_1^2 \nabla^2 \boldsymbol{\varepsilon} + \ell_2^4 \nabla^4 \boldsymbol{\varepsilon} = \boldsymbol{\varepsilon_0}. \tag{11}$$

The corresponding solution for the appropriate component of the dislocation density tensor is now obtained as

$$\alpha_z = (b_z / 2\pi)(1/c_1^2 - c_2^2)[K_0(r/c_1) - K_0(r/c_2)]; \quad c_1^2 + c_2^2 = \ell_1^2, \quad c_1^2 c_2^2 = \ell_2^4. \tag{12}$$

It then turns out that for $c_1 = c_2 = \ell_2$, we have

$$\alpha_z = \frac{b_z}{2\pi} \frac{r}{2\ell_2^3} K_1\left(\frac{r}{\ell_2}\right). \tag{13}$$

This suggests that for $r \to 0 \Rightarrow \alpha_z = b_z / (4\pi \ell_2^2)$, i.e. the relevant component of the dislocation density tensor is finite on the dislocation line. Figure 3 is borrowed from recent work of the author and his co-workers [4b]. It shows a good comparison between the predictions of Gradela and the experimental measurements, as depicted in the companion Table.

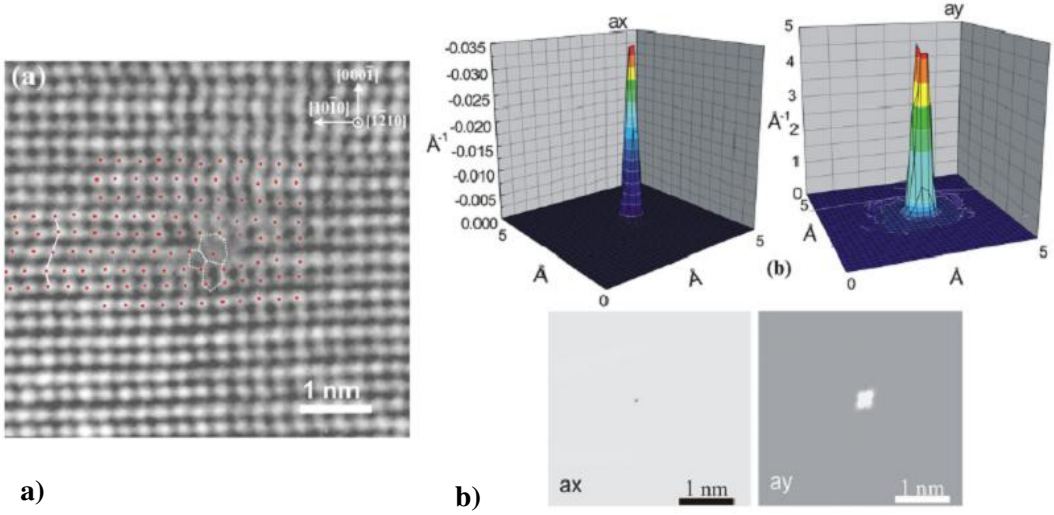

Figure 3: a) *HRTEM experimental image of an edge partial dislocation bounding a I1 SF (⟨1210⟩ projection). The intensity peaks corresponding to the positions of atomic columns have been marked with dots. The dislocation core (5/7- or 12-atom rings configuration) which has been identified by both GPA and peak finding is indicated; the stacking sequence . . . ABABCAC. . .across the SF is also indicated.* **b)** *Corresponding dislocation density tensor components a_x and a_y (3D representations and in-plane projections) obtained by GPA with $g = 10\bar{1}0$ and $g = 0002$, respectively, using masks of radius equal to g/4 around the Bragg spots in Fourier space*

Table: DDT Measurements - $\boldsymbol{\alpha} = \nabla \times \boldsymbol{\varepsilon}$

Dislocation core	5/7 ring (nm)	8 ring (nm)
Experimental	0.29	0.31
Calculated	0.25	0.31

6. X-ray Line Profile Analysis

The Fourier Transform (FT) of the line profile, designated by A(L), is given, according to Warren and Averbach [6], by the expression

$$\log A(L) = \log A_s(L) - 2\pi^2 g^2 L^2 \left\langle \varepsilon_L^2 \right\rangle \ , \tag{14}$$

where L is the Fourier variable, g is the absolute value of the diffraction vector and A_s is the size Fourier transform, while $\left\langle \varepsilon_L^2 \right\rangle$ denotes as usual the mean square strain. For random atomic displacements $\left\langle \varepsilon_L^2 \right\rangle$ is constant. For randomly distributed dislocations Krivoglaz and Ryaboshapka [7] obtained the expression

$$\left\langle \varepsilon_L^2 \right\rangle = \left(b/2\pi\right)^2 \pi\rho C \log\left(D/L\right), \tag{15}$$

i.e. the K-R formula valid for small L values only (D is the crystallite size, ρ is the dislocation density). Wilkens [8] improved the K-R formula by calculating the mean strain for the entire L range. The same logarithmic term as in the K-R formula holds but it does not diverge with crystallite size, depending on a correlation length parameter R_e^* outsize of which there is no dislocation interaction (R_e^* denotes the radius of a tube with dislocation density ρ).

According to the continuum theory for linear deformations, the longitudinal strain parallel to the direction of **g** is

$$\varepsilon_{\mathbf{g}}(L,\mathbf{r}) = \frac{1}{L}\left[\frac{\mathbf{g}}{|\mathbf{g}|}\mathbf{u}\left(\mathbf{r} + \frac{L}{2}\frac{\mathbf{g}}{|\mathbf{g}|}\right) - \frac{\mathbf{g}}{|\mathbf{g}|}\mathbf{u}\left(\mathbf{r} - \frac{L}{2}\frac{\mathbf{g}}{|\mathbf{g}|}\right)\right] = \frac{1}{L}\int_{-L/2}^{L/2} \frac{\mathbf{g}}{|\mathbf{g}|}\varepsilon\left(\mathbf{r} + s\frac{\mathbf{g}}{|\mathbf{g}|}\right)\frac{\mathbf{g}}{|\mathbf{g}|}\,ds \tag{16}$$

where **u** denotes displacement and $\boldsymbol{\varepsilon}$ strain, while the mean square strain is found from the relation

$$\left\langle \varepsilon_{\mathbf{g},L}^2 \right\rangle = \int_V \left[\varepsilon_{\mathbf{g}}(L,\mathbf{r})\right]^2 dV \Big/ \int_V dV \, . \tag{17}$$

In the case of the (100) reflection, we obtain

$$\varepsilon_{\mathbf{g}}(L,\mathbf{r}) = \frac{1}{L}\int_{-L/2}^{L/2} \varepsilon_{xx}\left(\mathbf{r} + s\mathbf{e}_x\right) ds \quad \text{for any } L \neq 0,$$

and (18)

$$\varepsilon_{\mathbf{g}}(0,\mathbf{r}) = \varepsilon_{xx}(\mathbf{r}) \qquad \text{for } L = 0 \, .$$

The strain function for edge dislocations can be computed by using Gradela (e.g. [2]). It turns out, in particular, that the ε_{xx} component of the strain tensor $\boldsymbol{\varepsilon}$ corresponding to an edge dislocation with Burgers vector $\mathbf{b} = b\,\mathbf{e}_x$ is

$$\varepsilon_{xx} = -\frac{b}{4\pi(1-\nu)} y \frac{(1-2\nu)r^2 + 2x^2}{r^4} + \frac{b}{2\pi(1-\nu)} y\left[\left(y^2 - \nu r^2\right)\Phi_1 + \left(3x^2 - y^2\right)\Phi_2\right], \tag{19}$$

where $\Phi_1 = \frac{1}{r^3\sqrt{c}} K_1\left(r/\sqrt{c}\right)$, $\Phi_2 = \frac{1}{r^4}\left[\frac{2c}{r^2} - K_2\left(r/\sqrt{c}\right)\right]$, $r^2 = x^2 + y^2$. Figure 4 depicts the variation of $\left\langle \varepsilon_L^2 \right\rangle$ with respect to logL as obtained through the classical model and a logarithmic approximation, through the gradient model, and through measurements for polycrystalline Cu. The crossing of the experimental curve over the Gradela curve is most likely due to the experimental uncertainty. The more accurate data shown in Figure 5 for a Cu single crystal result to an experimental curve which seems to have the same trends as the Gradela theoretical curve. The X-ray line profile for the deformed Cu single crystal given in Figure 5a depicts the measured line profile of the (111) reflection of a deformed single crystal Cu sample: the (count) intensity I is plotted as a function of $K - K_0$, where $K = (2\sin\theta)/\lambda$ and K_0 is the K value at the exact Bragg position. The intensity scale is logarithmic. The corresponding prediction from Gradela is given in Figure 5b, i.e. the mean square strain $\left\langle \varepsilon_L^2 \right\rangle$ as a function of logL, as determined experimentally for deformed Cu single crystal by FT. It is noted that $\left\langle \varepsilon_L^2 \right\rangle$ obtained this way is not singular, but it tends to a finite value for $L \to 0$. These and the rest of the results listed in this section, which are also reviewed in a recent article by the author and co-workers [9], will be discussed in detail in [10].

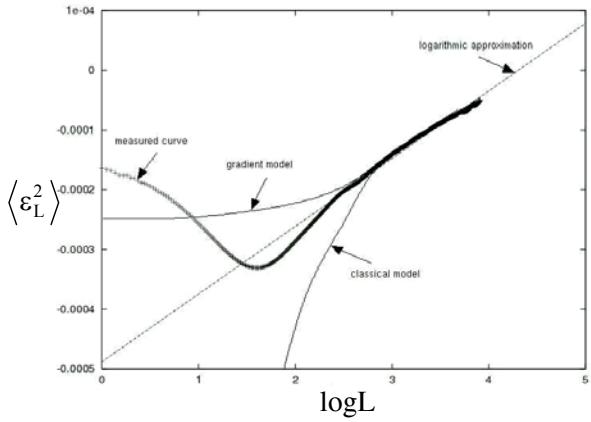

Figure 4: *Variations of* $\left\langle \varepsilon_L^2 \right\rangle$ *with respect to logL*

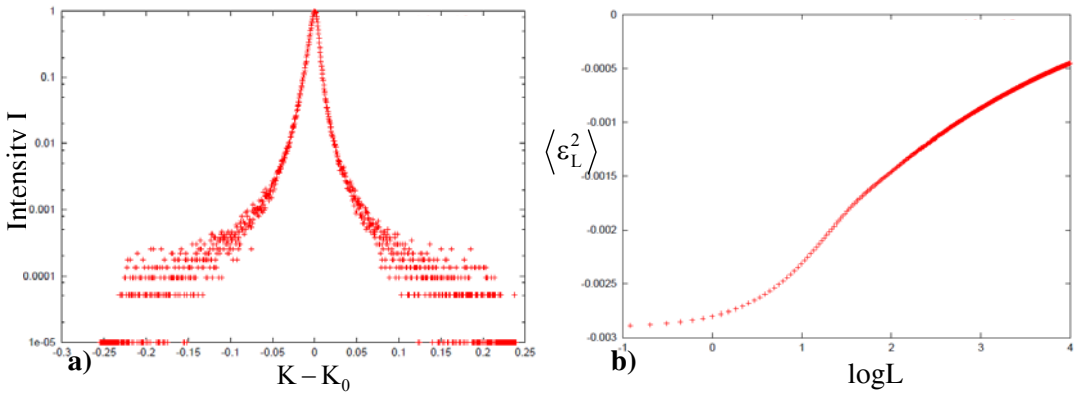

Figure 5: (a) *X-ray line profile for a deformed Cu single crystal determined experimentally;* **(b)** *Corresponding* $\left\langle \varepsilon_L^2 \right\rangle$ *graph determined theoretically from Gradela*

The results depicted in Figures 4 and 5 suggest that careful measurements seem to validate the predictions of Gradela. To support this further we provide in Figures 6 and 7 results pertaining to polycrystals with ultrafine grain size produced by the ECAP method. As already mentioned, some of these results are included in a recent article on applications of gradient theory [9], but an extended discussion focussing on the application of Gradela to X-ray line profile analysis is forthcoming [10] where details on the relevance of Figures 6 and 7 will be given.

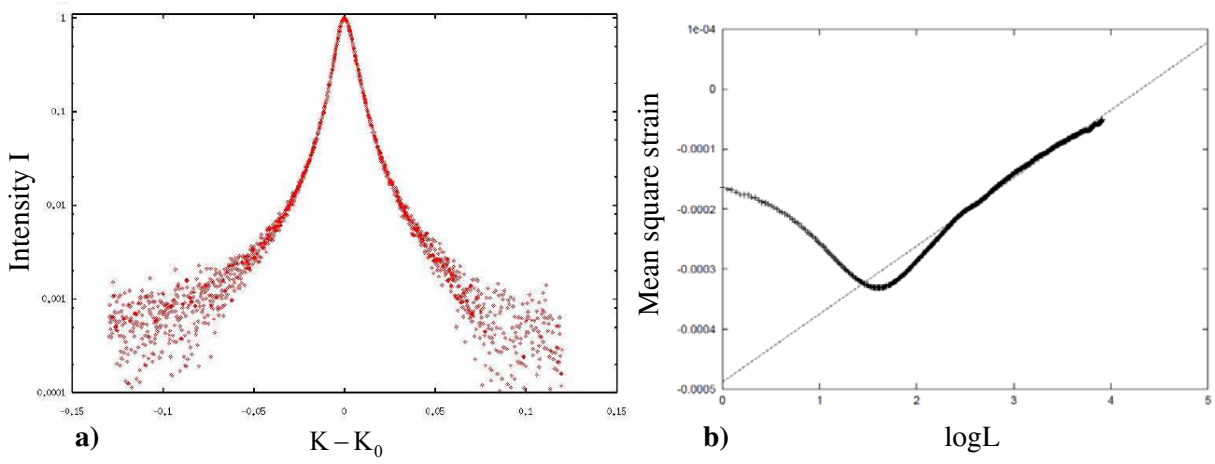

Figure 6: a) *X-ray line profile for ECAP Cu polycrystal;* **b)** *Corresponding* $\left\langle \varepsilon_L^2 \right\rangle$ *graph*

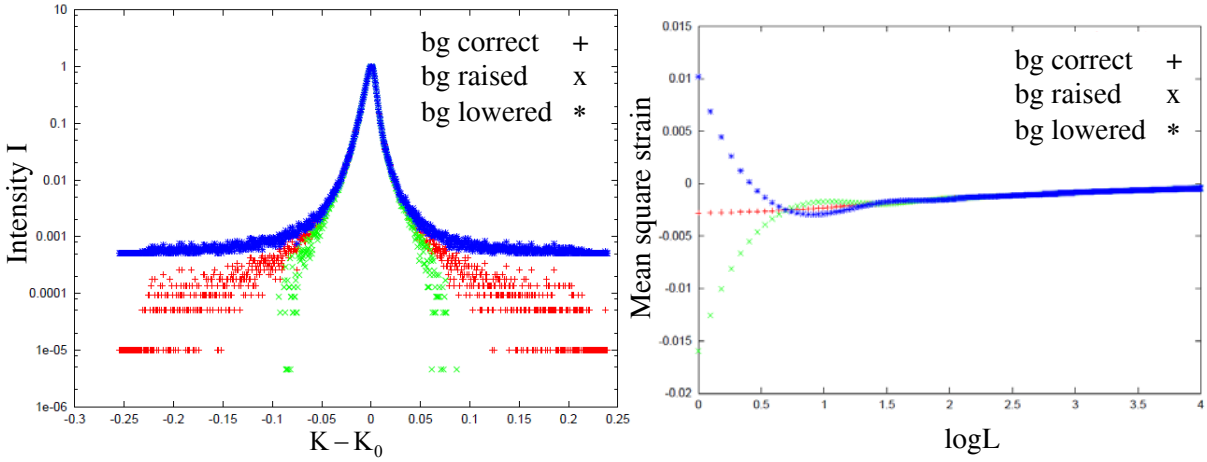

Figure 7: *The effect of Background (bg) I vs.* $K - K_0$ *data on the* $\left\langle \varepsilon_L^2 \right\rangle$ *vs. logL plots*

7. Revisiting Dislocation Theory

7.1. Other Non-singular Dislocation Models

It is pointed out that non-singular dislocation models have been proposed in the literature before. Reference is made, in particular, to the classical Peirls-Nabarro atomistic model, to Li's hollow dislocation model, and to a more recent Cai/Arsenlis/Weinberger/Bulatov dislocation core-spreading (or b-spreading) model [11].

It turns out that the shear stress $\sigma_{xy}(x,0)/[Gb/2(1-\nu)]$ on the glide plane under the assumption of same peak stress for these models varies according to the following distributions: $x/\left[x^2+(a^2/4(1-\nu)^2)\right]$ for the Peirls-Nabarro; $1/x-r_0^3/x^3$ for Li's; $1/x-4c/x^3+(2/x)\,K_2\left(x/\sqrt{c}\right)$ for Gradela; $x/(x^2+\alpha^2)$ for Cai/Arsenlis/Weinberger/Bulatov (CAWB) models (with $r_0\simeq 0.6a$, $\alpha=0.76a$ where a denotes the lattice parameter). A comparison between the aforementioned non-singular dislocation models is given in Figure 8a.

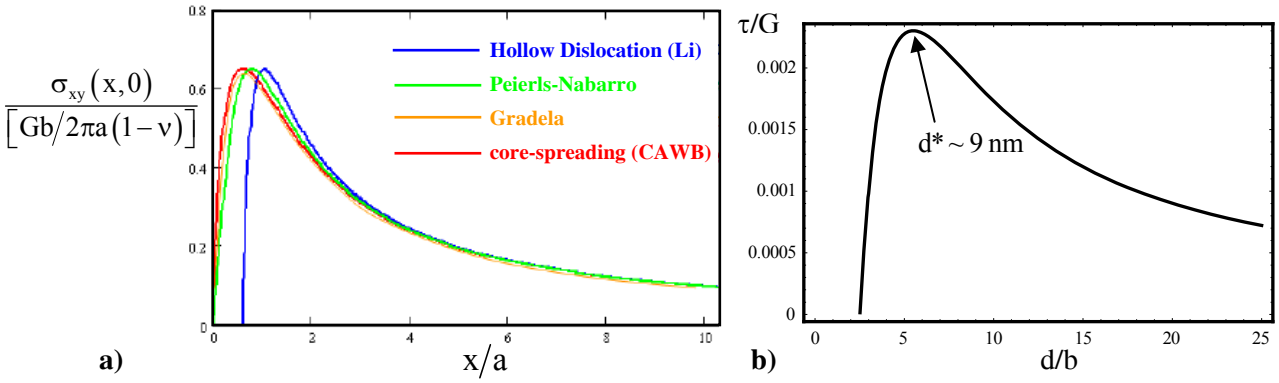

Figure 8: a) *Comparison of various non-singular dislocation models (for the same maximum stress);* **b)** *Qualitative plot of the dimensionless stress quantity* τ/G *over the dimensionless grain size quantity* d/b

7.2. Image Force – Inverse Hall Petch Behavior

By following the same procedure as in Section 4, the self-energy per unit length of a screw dislocation within the gradient theory of micro/nanoelasticity turns out to be given by the expression

$$W=\frac{Gb^2}{4\pi}\left[\ln\frac{R}{2\sqrt{c}}+\gamma^E+K_0\left(\frac{R}{\sqrt{c}}\right)\right], \tag{20}$$

where R is the radial coordinate defining the material volume surrounding the dislocation line considered, γ^E is the Euler constant, K_0 denotes the appropriate Bessel function, and the rest of the symbols have their usual meaning. It is emphasized again that the self-energy is not singular as in classical elasticity and the necessity of introducing an arbitrary dislocation core parameter for dispensing with such singularity is eliminated. In fact, the gradient coefficient c (its square root denotes the relevant material internal length) provides a new possibility to account for dislocation core effects as discussed in previous sections, as well as in [2] and the related bibliography listed therein.

On using the above gradient modification of the self-energy in conjunction with a standard image force argument advanced in [12] (see also [13]) based on classical elasticity theory, we obtain the following relation

$$\tau b=\frac{Gb^2}{2\pi}\left[\frac{1}{d}-\frac{1}{2\sqrt{c}}K_1\left(\frac{d}{2\sqrt{c}}\right)\right], \tag{21}$$

for a dislocation sitting at the center of a grain of diameter d; the second term of the l.h.s. involving the Bessel function is due to the gradient elasticity effect.

The (qualitative) plot of the dimensionless stress quantity τ/G over the dimensionless grain size quantity d/b (Figure 8b) has a rising and a descending branch with a maximum occurring at a critical grain size at the nanometer regime. Thus, in principle, this plot may be used for establishing another

interesting interpretation of the "standard" and "inverse" Hall-Petch behavior as it will be discussed elsewhere.

Acknowledgements
The support of EC under RTN–DEFINO HPRN-CT-2002-00198 and of the US National Science Foundation under NIRT Program (NIRT Grant DMI-0532320) is acknowledged. The support of the Greek Government under the PENED and PYTHAGORAS programs is also acknowledged. Useful discussions and the generous cooperation with the Electron Microscopy Laboratory of Aristotle University headed by Professor Th. Karakostas is gratefully acknowledged. The same holds for the X-ray line profile analysis group of Eotvos University headed by Professor T. Ungar. Useful discussions with I. Konstantopoulos, J. Kioseoglou and G.Ribarik (all post-graduate researchers supported by the aforementioned projects) are gratefully acknowledged, along with the assistance of my colleague A. Konstantinidis who checked the manuscript and made helpful suggestions.

References

[1] E.C. Aifantis, On the role of gradients in the localization of deformation and fracture, Int. J. Engrg. Sci. 30 (1992) 1279-1299.
[2] E.C. Aifantis, Update on a class of gradient theories, Mech. Mater. 35 (2003) 259-280.
[3] C.Q. Ru and E.C. Aifantis, A simple approach to solve boundary value problems in gradient elasticity, Acta Mechanica 101 (1993) 59-68 (1993).
[4] J. Kioseoglou, G.P. Dimitrakopulos, Ph. Komninou, Th. Karakostas, I. Konstantopoulos, M. Avlonitis and E.C. Aifantis, Analysis of partial dislocations in wurtzite GaN using gradient elasticity, Phys. Status Solidi A 203 (2006) 2161-2166. [see also: J. Kioseoglou, G.P. Dimitrakopulos, Ph. Komninou, Th. Karakostas and E.C. Aifantis, Dislocation core investigation by geometric phase analysis and the dislocation density tensor, J. Physics D: Appl. Physics 41 (2008) 035408/1-8; J. Kioseoglou, G.P. Dimitrakopulos, Ph. Komninou and Th. Karakostas, Atomic structures and energies of partial dislocations in wurtzite GaN, Phys. Rev. B 70 (2004) 035309/1-12.]
[5] L. Verlet, Computer "experiments" on classical fluids. I. Thermodynamical properties of Lennard-Jones molecules, Phys.Rev. 159 (1967) 98-103.
[6] B.E. Warren and B.L. Averbach, The Separation of cold-work distortion and particle size broadening in X-ray patterns J. Appl. Phys. 23 (1952) 497-498.
[7] M.A. Krivoglaz and K.P. Ryaboshapka, Theory of scattering of X-rays and thermal neutrons by real crystals, Fizika Metall. 15 (1963) 18-31.
[8] M. Wilkens, Theoretical aspects of kinematical X-ray diffraction profiles from crystals containing dislocation distributions, in: Fundamental Aspects of Dislocation Theory, J.A. Simmons, R. deWit and R. Bullough (Eds.), Vol. II, pp. 1195-1221, Nat. Bur. Stand. (USA) Spec. Publ. No. 317., Washington, DC, USA (1970).
[9] J. Kioseoglou, I. Konstantopoulos, G. Ribarik, G.P. Dimitrakopulos and E.C. Aifantis, Nonsingular dislocation and crack fields: Implications to small volumes, Microrsyst. Technol. 15 (2009) 117-121.
[10] G. Ribarik, T. Ungar and E.C. Aifantis, X-ray line profile analysis through gradient elasticity, forthcoming.
[11] W. Cai, A. Arsenlis, C.R. Weinberger and V.V. Bulatov, A non-singular continuum theory of dislocations, J. Mech. Phys. Solids 54 (2006) 561-587.
[12] E.C. Aifantis, W.W. Milligan and S.A. Hackney, Final AFOSR Report (F 49620-95-1-0208 & F 49620-94-1-0255), 2000.
[13] S. Hackney, M. Ke, W.W. Milligan and E.C. Aifantis, Grain size and strain rate effects on the mechanisms of deformation and fracture in nanostructured metals, in: Processing and Properties of Nanocrystalline Materials, C. Suryanarayana et al (Eds.), pp. 421-426, TMS, Warrendale, PA (1996).